How Viscous is the Solid-like Structure at the Interface of Ionic Liquids? A Study Using Total Internal Reflection Fluorescence Spectroscopy with a Fluorescent Molecular Probe Sensitive to High Viscosity

Naoya Nishi,*,† Takashi Yamazawa,† Tetsuo Sakka,† Hiroki Hotta,‡ Takayuki Ikeno,¶ Kenjiro Hanaoka,¶ and Hiromi Takahashi§

†*Department of Energy and Hydrocarbon Chemistry, Graduate School of Engineering, Kyoto University, Kyotodaigakukatsura, Nishikyo-ku, Kyoto 615-8510, Japan*

‡*Graduate School of Maritime Sciences, Kobe University, 5-1-1 Fukaeminami-machi, Higashinada-ku, Kobe 658-0022, Japan*

¶*Graduate School of Pharmaceutical Sciences, The University of Tokyo, 7-3-1 Hongo, Bunkyo-ku, Tokyo 113-0033, Japan*

§*System Instruments Co., Ltd, 776-2, Komiya-machi, Hachioji, Tokyo 192-0031, Japan*

E-mail: nishi.naoya.7e@kyoto-u.ac.jp

Abstract

Aiming at the evaluation of the viscosity of the interfacial solid-like structure of ionic liquids (ILs), we performed total internal reflection fluorescence (TIRF) spectroscopy for N,N-diethyl-N'-phenyl-rhodamine (Ph-DER), a fluorescent probe that is sensitive to viscosity in a high viscosity range. TIRF spectra at the glass interface of trioctylmethylammonium bis(nonafluorobutanesulfonyl)amide (TOMAC4C4N), a hydrophobic IL, showed that the fluorescence intensity of Ph-DER increases with decreasing the evanescence penetration depth, suggesting that there exists a high-viscosity region at the interface. In contrast, glycerol, which is a molecular liquid with a bulk viscosity similar to TOMAC4C4N, did not show such a fluorescence increase, supporting that the formation of a highly-viscous solid-like structure at the interface is intrinsic to ILs. A model analysis suggested that the high viscous region at the glass interface of TOMAC4C4N is at least twice thicker than the ionic multilayers at the air interface, implying that the solid substrate enhances the ordering of the interfacial structure of ILs. The viscosity at the glass interface of TOMAC4C4N was found to be at least 40 times higher than the liquid bulk.

Introduction

Ionic liquids (ILs) are low-melting-point salts composed of cations and anions with a wide potential window, non-volatility, flame resistance, and ionic conductivity.[1] Because of these features, ILs are promising candidates as alternative electrolytes in lithium-ion batteries and electric double-layer capacitors.[2,3] Since the interfacial structure dynamics of ILs greatly affects the rate of redox reactions and mass transfer, it is important to understand the interfacial structure dynamics in order to apply ILs to electrochemical devices.[4] In our previous study using X-ray reflectometry (XR), a multi-layered ordering structure was revealed at the gas interface of an ionic liquid, trioctylmethylammonium bis(nonafluorobutanesulfonyl)amide (TOMAC4C4N).[5] The study was followed by subsequent XR studies at the gas interface[6–11] and the water interface[8,12] of various ILs, confirming the generality of the characteristic of ILs to form ionic multilayers even at the soft interfaces without the help of solid substrates. At the solid interface of ILs, studies using XR,[13–17] atomic force microscopy (AFM),[18–20] and surface force apparatus (SFA)[21–23] confirmed the existence of ionic multilayers and furthermore AFM and SFA studies unveiled that the layers are highly viscous and solid-like. Molecular dynamics (MD) simulation studies illustrated that intra-layer diffusion of ions in the ionic multilayers are slower than the bulk counterpart[18,24–28] and inter-layer diffusion is further slower,[25,29] sometimes unevaluable[18,27] on the time scale of simulation. Electrochemical impedance spectroscopy[30–36] and other electrochemical techniques[37,38] found strong potential hysteresis and ultraslow process in the ion dynamics at the electrode interface of ILs. The potential hysteresis has also been observed in sum frequency generation,[39] surface enhanced infrared absorption spectroscopy,[40–42] and XR.[15] Also, XR[16,17,43] and electrochemical surface plasmon resonance (ESPR)[44–46] showed a slow relaxation of the interfacial structure of ILs, including TOMAC4C4N,[44] on the order of seconds that cannot be explained by bulk properties.

It would be invaluable if we could evaluate the viscosity of the interfacial solid-like structure of ILs. In fact, SFA studies reported that the shear viscosity of ILs measured using two

atomically flat solid substrates exponentially increases when the inter-substrate distance is narrowed below 10 nm.[21,22] However, a recent AFM study proposes that such a confined situation between two solid walls induce a dramatic change of ILs to a solid-like phase.[20] To investigate the interfacial viscosity as an intrinsic characteristic of ILs, a study at the soft interfaces or at least at the one-solid open (not confined) interface would be desirable.

In the present study, in order to evaluate the interfacial viscosity of ILs, we adopted another approach, that is, total internal reflection fluorescence (TIRF) spectroscopy with a viscosity-sensitive fluorescent molecular probe. TIRF is a powerful technique sensitive and selective to fluorescent molecules on the interface[47,48] and applied to time-resolved measurements for inter-molecular energy transfer[49] and molecular reorientation dynamics[50,51] and imaging measurements for bio-sensing and cell analysis.[52,53] In the present study, TOMAC4C4N, for which we previously studied the interfacial structure[5,41] and dynamics,[37,41,44,54–57] was chosen as an IL to be investigated. *N*, *N*-diethyl-*N*'-phenyl-rhodamine (Ph-DER,[58] see Fig.S1a for the structure) was used as a probe whose fluorescence intensity is sensitive to the viscosity even for highly viscous liquids like TOMAC4C4N. Ph-DER is one of rhodamine derivatives that have a phenyl moiety attached to one of the rhodamine nitrogen atoms. Ph-DER shows a viscosity sensitivity in a high viscosity range, as was observed for other aryl-substituted rhodamine dyes.[59,60] By using Ph-DER in TIRF spectroscopy we explored the interfacial viscosity of TOMAC4C4N.

Experimental

TOMAC4C4N (refractive index, $n_{\rm l} = 1.411$ at 532 nm) was prepared and purified as described previously.[54,61] Glycerol ($n_{\rm l} = 1.474$ at 532 nm), as a molecular solvent with a viscosity similar to TOMAC4C4N for comparison, was used as purchased (Nacalai Tesque). The viscosity, η, of TOMAC4C4N, glycerol, and other liquids was measured using a viscometer (TVE-22, Toki Sangyo). The η values for TOMAC4C4N and glycerol were measured to

be 2000 and 1300 mPa s at 20°C, respectively. Ph-DER was synthesized[58] and dissolved in TOMAC4C4N and glycerol. Rhodamine B (Wako, hydrochloride salt), whose structure is shown in Fig.S1b, was also added to the liquids as an internal reference dye.

TIRF spectra for Ph-DER and RB at the glass interface of the liquids were measured using a slab optical waveguide spectrometer (SIS-5100, System Instruments). A schematic diagram of the experimental setup is shown in Fig.S1c. A glass plate (K-LaSFn1, Sumita Optical Glass; refractive index, $n_{\mathrm{g}} = 1.813$ at 532 nm) was used as a slab optical waveguide. The glass plate was mounted on an xy stage whose surface is micro-roughened to prevent attenuation of the beam on the back surface of the glass plate. Just before measurements, the glass surface was cleaned by chemical etching with a saturated ethanol solution of KOH, followed by washing with methanol and drying in air. A liquid drop of the dye solutions was placed on the surface of the glass plate. A diode-pumped solid-state laser (LCX-532S-300-CSB-PPF, Oxxius) was mounted on a goniometer arm, which enabled us to finely adjust the incident angle. A beam with a wavelength, λ, of 532 nm from the laser was introduced from the polished edge surface of the glass plate. The laser beam propagated in the glass plate by repeated TIR and generated the evanescent wave on the liquid side of the glass/liquid interface. The evanescence penetration depth, δ, can be written as,

$$\delta = \frac{\lambda}{2\pi\sqrt{n_{\mathrm{g}}^2 \sin^2\theta - n_{\mathrm{l}}^2}} \tag{1}$$

where n_{g} and n_{l} are the refractive indices of the glass and a liquid at 532 nm and θ is the incidence angle of the laser at the glass/liquid interface (Fig.S1c). It should be noted that eq 1 is derived without taking into account the existence of the solid-like ionic multilayers at the interface, which can have moderately higher n than the bulk IL.[62,63] However, the existence of such interfacial layers with a molecular-level thickness causes a negligible change in the local electric field and the penetration depth of evanescent wave. Fluorescence from dyes

excited by the evanescent wave was collected with a lens and detected by a spectrometer (USB2000, Ocean Optics). No matching oil was required in this arrangement and the incident angle was extremely reproducible and finely adjusted by the goniometer.

By evaluating the relative fluorescence intensity of Ph-DER with respect to RB, $\bar{I}_{\mathrm{F}}$, we canceled out θ dependent instrumental function and was able to focus on the interfacial viscosity of the liquids. This is possible because Ph-DER is sensitive to the viscosity on the order of 1000 mPa s whereas the fluorescence intensity of RB is saturated at this high viscosity range (Fig.3). The fluorescence spectrum of each dye in each liquid was separately measured at $\theta = 63°$, which was used to evaluate $\bar{I}_{\mathrm{F}}$ in the liquids at various δ by using classical least squares (CLS).

Experimental $\bar{I}_{\mathrm{F}}$ data depending on δ was fitted with a model function of the fluorescence quantum yield $\phi_{\mathrm{F}}(z)$ around the interface which can be different from that in the bulk, $\phi_{\mathrm{F,bulk}}$. The model, the so-called one-box model, assumes a uniform interfacial layer with a thickness of d. The model function is written as

$$\bar{I}_{\mathrm{F}}(\delta) = \frac{I_{\mathrm{Ph-DER}}}{I_{\mathrm{ref}}} = k\frac{\int_0^\infty \bar{\phi}_{\mathrm{F}}(z)\left(E_0 e^{-z/\delta}\right)^2 \mathrm{d}z}{\int_0^\infty \left(E_0 e^{-z/\delta}\right)^2 \mathrm{d}z} \tag{2}$$

with

$$\bar{\phi}_{\mathrm{F}}(z) = \begin{cases} f & (0 \le z \le d) \\ 1 & (d \le z) \end{cases}$$

where the z axis represents the surface normal direction with $z = 0$ at the interface and $z > 0$ in the liquid, E_0 is the electric field intensity of the evanescent wave at the interface, $E_0 e^{-z/\delta}$ indicates that the electric field decays as it is further away from the interface, k is a constant that represents the fluorescence intensity ratio in the IL bulk ($\lim_{\delta\to\infty} \bar{I}_{\mathrm{F}}(\delta) = k$), $\bar{\phi}_{\mathrm{F}} = \phi_{\mathrm{F}}/\phi_{\mathrm{F,bulk}}$, and f is the fluorescence quantum yield in the interfacial layer normalized

with the bulk counterpart. The denominator in eq 2 does not have the $\bar{\phi}_{\mathrm{F}}$ term because the fluorescence intensity of RB is not viscosity sensitive in the viscosity range investigated in the present study (Fig.3). In the model, we assumed no effect of adsorption of dyes on the glass surface, which was confirmed to be valid from control experiments (see Results and Discussion below). Also, it is possible that the Ph-DER concentration in the solid-like ionic multilayers is different from that in the bulk IL. However, what we analyze is not the absolute fluorescent intensity of Ph-DER but the fluorescent intensity ratio of two dyes (Ph-DER and RB) that share the same rhodamine structure (Fig.S1a,b). Therefore, these two dyes would have similar partition behavior between the bulk IL and the ionic multilayers. Possible accumulation or depletion effect in the ionic multilayers is largely canceled out in the fluorescent intensity ratio. Eq 2 can be calculated as,

$$\bar{I}_{\mathrm{F}} = k\left\{f + (1-f)\exp(-2d/\delta)\right\} \tag{3}$$

Here we assume that $2d/\delta \ll 1$ because d is on the order of the ion size and δ is on the order of wavelength, and then

$$\bar{I}_{\mathrm{F}} = k\left\{1 + \frac{2d(f-1)}{\delta}\right\} \tag{4}$$

This equation was fitted to the experimental $\bar{I}_{\mathrm{F}}$ vs. δ^{-1} plots to evaluate the parameters. Unfortunately, this equation shows that we cannot separately evaluate d and f. This is because the evanescent field is significantly thicker than the interfacial layer. Nevertheless, if we reasonably estimate d, we can evaluate f semi-quantitatively.

Results and Discussion

TIRF spectra of Ph-DER and RB in TOMAC4C4N are shown in Fig.1a. Single fluorescence peaks are discernible in the spectra at around 577 nm. These peak positions are between

572 and 589 nm that are the peak wavelength for fluorescence spectra (Fig.1b) for RB and Ph-DER alone dissolved in TOMAC4C4N, respectively. This indicates that the single peaks in Fig.1a are actually composed of two peaks from the two dyes. The fluorescence intensity decreases with decreasing δ. This tendency is as expected because thinner evanescent field leads to less fluorescent dyes excited. A closer look at the spectra in Fig.1a finds the redshift of the peaks with decreasing δ. This is more obvious in Fig.1c, which are the spectra already shown in Fig.1a but normalized with individual peak height to ease the comparison, and also in Fig.S3a where the peak wavelength is plotted as a function of δ. The redshift implies that the relative contribution of two dyes to the "single" peak is changing, i.e., Ph-DER that fluoresces at longer wavelength increases its relative contribution with decreasing δ. Combined with the fact that smaller δ corresponds to more surface contribution, this behavior indicates that Ph-DER emits more fluorescence at the interface of TOMAC4C4N than in the liquid bulk. Because Ph-DER is a viscosity sensitive fluorescent probe, this suggests the existence of a high-viscosity region at the glass interface of TOMAC4C4N. This agrees with previous studies that reported ultraslow interfacial dynamics at the electrochemical interface of TOMAC4C4N.[37,44,54–57]

To compare with the behavior observed for TOMAC4C4N, which is an IL, we performed the same measurements for glycerol, which is a molecular liquid and has a viscosity similar to TOMAC4C4N (1300 and 2000 mPa s at 20°C, respectively). Fig.S2 shows TIRF spectra in glycerol. Glycerol exhibited the same tendency: smaller fluorescence intensity at smaller δ and peaks at around 582 nm (Fig.S2a) that is in between 577 and 589 nm for the corresponding 1-component spectra (Fig.S2b). However, in stark contrast to the case with TOMAC4C4N, the peak position remained almost unchanged for glycerol (Fig.S2c and Fig.S3b), suggesting that no Ph-DER fluorescence enhancement occurs at the glass interface of glycerol.

To quantitatively discuss the relative fluorescence intensity change, we extracted the relative contribution of the two dyes from the spectra using CLS. The extracted relative

fluorescence intensity, $\bar{I}_{\mathrm{F}}$, for TOMAC4C4N is shown in Figure 2. $\bar{I}_{\mathrm{F}}$ increased with decreasing δ, as qualitatively discussed above. For glycerol (Fig.S4), in contrast, the fluorescence intensity ratio was constant with respect to δ, which agrees with no peak shift observed in the spectra (Fig.S2c and Fig.S3b). This indicates that the viscosity of glycerol does not change at the interface.

A question is, does possible adsorption of Ph-DER and RB at the glass interface affect $\bar{I}_{\mathrm{F}}$ at small δ? A clean glass surface has silanol groups that may attract these dyes on the surface, although such an attraction should also work more or less onto IL ions (TOMA^+ and $\mathrm{C4C4N}^-$) and glycerol molecules. If the concentration of either or both of Ph-DER and RB at the interface is different from that in the bulk we would see δ dependence of $\bar{I}_{\mathrm{F}}$ irrespective to the viscosity change. To answer this question, we performed control experiments by using a glass plate whose surface is silanized to cap silanol groups with methyl groups. The glass was soaked in a hexane solution of chlorotrimethylsilane (10wt%) to silanize the surface. The $\bar{I}_{\mathrm{F}}$ vs δ^{-1} from the control experiments are shown in Fig.S5. In both cases for TOMAC4C4N and glycerol, the behavior was the same as without the silanization treatment, illustrating that the adsorption effect is negligible. A possible explanation is that the attraction to surface silanol groups is similar for the dyes, IL ions, and glycerol. Also, a thin water layer may cover the glass surface even in organic solvents[64] and TOMAC4C4N, a hydrophobic IL, preventing the approach of any other ions and molecules onto the glass surface.

To obtain the information on the extent that the viscosity of TOMAC4C4N increases at the interface, we fitted eq 4 from the one-box model to the $\bar{I}_{\mathrm{F}}$ vs δ^{-1} plot with k and $d(f-1)$ as fitting parameters. The obtained parameters are $k = 0.86 \pm 0.11$ and $d(f-1) = 72 \pm 16$ nm. The f value contains the interfacial viscosity information because Ph-DER is a viscosity fluorescent probe. ϕ_{F} ($= f\phi_{\mathrm{F,bulk}}$) can be related to η by making a calibration curve between these parameters. The calibration curve was obtained by determining ϕ_{F} for Ph-DER in three liquids (TOMAC4C4N, glycerol, and ethylene glycol) and at several temperatures (5-50°C with an increment of 5°C) with a relative method[65] using $\phi_{\mathrm{F}} = 0.65$ for RB in ethanol

as a standard value. At the temperatures other than 20°C, ϕ_{F} in a liquid was evaluated by using the value in the liquid at 20°C as a reference. In other words, we neglected the temperature dependences of density, molar absorption coefficient, and refractive index, which will cause minor effects on the calibration curve. Fig.3 shows $\log \phi_{\mathrm{F}}$ vs $\log \bar{\eta}$ plots, where $\bar{\eta} = \eta/\eta_{\mathrm{TOMAC4C4N,bulk}}$. The ϕ_{F} for TOMAC4C4N at 20°C, which is $\phi_{\mathrm{F,bulk}}$, was determined to be 0.145. From the linear regression using least squares, we obtained the parameters in the Förster-Hoffman type equation[66] $\log \phi_{\mathrm{F}} = \log a_0 + a_1 \log(\bar{\eta})$: $a_0 = 0.114 \pm 0.005$ and $a_1 = 0.598 \pm 0.013$. $a_1 = 0.6$ is a typical value for fluorescence dyes;[59,60,66] even RB shows $a_1 \sim 0.6$ viscosity dependence,[67] but at low viscosity regime, ∼1 mPa s, much lower than the order of 1000 mPa s for the liquids in the present study. ϕ_{F} for RB is saturated at unity over 10 mPa s[68] as shown as open diamond in Fig. 3 and that is why we can use RB as an internal reference dye that does not show viscosity dependence in the present study. With all the relations between d and f, between f and ϕ_{F}, and between ϕ_{F} and $\bar{\eta}$ altogether, we finally obtained a relation between d and $\bar{\eta}$ as follows (see Supporting Information for the derivation)

$$\bar{\eta} = 1.5 \left(1 + \frac{72}{d/\mathrm{nm}}\right)^{1.67} \tag{5}$$

Here we do not know the exact value of d, but it is worth to put a plausible value into eq 5. In our previous x-ray reflectivity study on the air interface of TOMAC4C4N, we revealed that there are ionic multilayers formed with several layers where each layer has a thickness of 1.5 nm, corresponding to the ionic size.[5] If we say the number of layers is four, as can be estimated from the electron density profile at the air interface of TOMAC4C4N, d would be 6.0 nm and from eq 5 $\bar{\eta}$ is estimated to be 109. This value is significantly high and a solid-like layering structure reported at the interface of several kinds of IL[19,23] would have such a high viscosity. But the $\bar{\eta}$ value of 109 has a problem when looking at Fig.3. The vertical axis of Fig.3 is a logarithmic scale of fluorescence quantum yield and it should not

exceed zero, i.e., the upper limit of ϕ_F is naturally unity. This upper limit in ϕ_F leads to an upper limit to $\bar{\eta}$, which is $\bar{\eta} = 38 \pm 6$ at $\phi_F = 1$ in the calibration curve in Fig.3. Therefore this viscosity fluorescent probe Ph-DER cannot detect the relative viscosity higher than 40 for TOMAC4C4N and the fluorescence signal will be saturated. By going back to eq 5 and inserting $\bar{\eta} = 38$, we estimate the lower limit of d, which is 12 nm. This thickness corresponds to 8 ionic layers for the TOMAC4C4N case and is twice as thick as what we found at the air interface of TOMAC4C4N. Solid substrates are known to enhance the structuring of ILs and also liquid molecules at the interface. For example, 13 ionic layers are found to be in a solid-like structure at the mica interface of 1-ethyl-3-methylimidazolium bis(trifluoromethanesulfonyl)amide,[23] while no ionic multilayers detectable via XR have been reported at the air interface.[10] TOMAC4C4N is likely to form ionic multilayers at the glass interface at least twice thicker than at the air interface. Our previous study using ESPR as a probe of the interfacial structure relaxation against the electrode potential change revealed that the relaxation time constant is three orders of magnitude longer than RC constant estimated from bulk conductivity and the interfacial capacitance.[44] That implies that the interfacial viscosity is three orders of magnitude higher than the bulk viscosity; $\bar{\eta} \sim 10^3$ and $\eta \sim 10^6$ mPa s at the interface. A liquid having such high viscosity may be categorized into semi-solids rather than liquid, which agrees with the results reporting the existence of a solid-like interfacial structure of ILs. A fluorescent probe that is sensitive to viscosity at higher viscosity range would be interesting to be used for future study.

Conclusions

A strategy using TIRF spectroscopy combined with a viscosity-sensitive fluorescent probe successfully detected the enhancement of interfacial viscosity at the interface of an IL. Although precise evaluation of the interfacial viscosity is impossible due to intrinsically lower spatial resolution of this method compared with the scale of the interfacial structure, a

semi-quantitative evaluation was still valid.

Acknowledgement

This work was partly supported by Grant-in-Aid for Scientific Research (No. 18K05171) and Kato Foundation for Promotion of Science.

Supporting Information Available

Supporting Information: The Supporting Information is available free of charge on the ACS Publications website at DOI: ***.

Structure of dyes; schematics for the experimental setup; TIRF spectra for glycerol; peak wavelength vs δ plots; I_{F} vs δ^{-1} plots for glycerol and those for TOMAC4C4N and glycerol at the silanized glass interface; the derivation of eq 5.

References

(1) Hayes, R.; Warr, G. G.; Atkin, R. Structure and Nanostructure in Ionic Liquids. *Chem. Rev.* **2015**, *115*, 6357–6426.

(2) Watanabe, M.; Thomas, M. L.; Zhang, S.; Ueno, K.; Yasuda, T.; Dokko, K. Application of Ionic Liquids to Energy Storage and Conversion Materials and Devices. *Chem. Rev.* **2017**, *117*, 7190–7239.

(3) Yang, Q.; Zhang, Z.; Sun, X.-G.; Hu, Y.-S.; Xing, H.; Dai, S. Ionic Liquids and Derived Materials for Lithium and Sodium Batteries. *Chem. Soc. Rev.* **2018**, *47*, 2020–2064.

(4) Wang, Y.-L.; Li, B.; Sarman, S.; Mocci, F.; Lu, Z.-Y.; Yuan, J.; Laaksonen, A.; Fayer, M. D. Microstructural and Dynamical Heterogeneities in Ionic Liquids. *Chem. Rev.* **2020**, *120*, 5798–5877.

(5) Nishi, N.; Yasui, Y.; Uruga, T.; Tanida, H.; Yamada, T.; Nakayama, S.; Matsuoka, H.; Kakiuchi, T. Ionic Multilayers at the Free Surface of an Ionic Liquid, Trioctylmethylammonium Bis(nonafluorobutanesulfonyl)amide, Probed by X-ray Reflectivity Measurements. *J. Chem. Phys.* **2010**, *132*, 164705(1–6).

(6) Nishi, N.; Uruga, T.; Tanida, H.; Kakiuchi, T. Temperature Dependence of Multilayering at the Free Surface of Ionic Liquids Probed by X-ray Reflectivity Measurements. *Langmuir* **2011**, *27*, 7531–7536.

(7) Mezger, M.; Ocko, B. M.; Reichert, H.; Deutsch, M. Surface Layering and Melting in an Ionic Liquid Studied by Resonant Soft X-ray Reflectivity. *Proc. Natl. Acad. Sci. U. S. A.* **2013**, *110*, 3733–3737.

(8) Nishi, N.; Uruga, T.; Tanida, H. Potential Dependent Structure of an Ionic Liquid at Ionic Liquid/Water Interface Probed by X-ray Reflectivity Measurements. *J. Electroanal. Chem.* **2015**, *759*, 129–136.

(9) Mars, J.; Hou, B.; Weiss, H.; Li, H.; Konovalov, O.; Festersen, S.; Murphy, B. M.; Rütt, U.; Bier, M.; Mezger, M. Surface Induced Smectic Order in Ionic Liquids - an X-ray Reflectivity Study of $[C_{22}C_1im]^+[NTf_2]^-$. *Phys. Chem. Chem. Phys.* **2017**, *19*, 26651–26661.

(10) Haddad, J.; Pontoni, D.; Murphy, B. M.; Festersen, S.; Runge, B.; Magnussen, O. M.; Steinruck, H.-G.; Reichert, H.; Ocko, B. M.; Deutsch, M. Surface Structure Evolution in a Homologous Series of Ionic Liquids. *Proc. Natl. Acad. Sci. U. S. A.* **2018**, *115*, E1100–E1107.

(11) Pontoni, D.; Haddad, J.; Murphy, B. M.; Festersen, S.; Konovalov, O.; Ocko, B. M.; Deutsch, M. Surface Phases and Surface Freezing in an Ionic Liquid. *J. Phys. Chem. C* **2019**, *123*, 3058–3066.

(12) Katakura, S.; Amano, K.-i.; Sakka, T.; Bu, W.; Lin, B.; Schlossman, M. L.; Nishi, N. Evolution and Reversible Polarity of Multilayering at the Ionic Liquid/Water Interface. *J. Phys. Chem. B* **2020**, *124*, 6412–6419.

(13) Mezger, M.; Schröder, H.; Reichert, H.; Schramm, S.; Okasinski, J. S.; Schöder, S.; Honkimäki, V.; Deutsch, M.; Ocko, B. M.; Ralston, J.; Rohwerder, M.; Stratmann, M.; Dosch, H. Molecular Layering of Fluorinated Ionic Liquids at a Charged Sapphire (0001) Surface. *Science* **2008**, *322*, 424–428.

(14) Zhou, H.; Rouha, M.; Feng, G.; Lee, S. S.; Docherty, H.; Fenter, P.; Cummings, P. T.; Fulvio, P. F.; Dai, S.; McDonough, J.; Presser, V.; Gogotsi, Y. Nanoscale Perturbations of Room Temperature Ionic Liquid Structure at Charged and Uncharged Interfaces. *ACS Nano* **2012**, *6*, 9818–9827.

(15) Uysal, A.; Zhou, H.; Feng, G.; Lee, S. S.; Li, S.; Fenter, P.; Cummings, P. T.; Fulvio, P. F.; Dai, S.; McDonough, J. K.; Gogotsi, Y. Structural Origins of Potential Dependent Hysteresis at the Electrified Graphene/Ionic Liquid Interface. *J. Phys. Chem. C* **2014**, *118*, 569–574.

(16) Chu, M.; Miller, M.; Douglas, T.; Dutta, P. Ultraslow Dynamics at a Charged Silicon-Ionic Liquid Interface Revealed by X-ray Reflectivity. *J. Phys. Chem. C* **2017**, *121*, 3841–3845.

(17) Reichert, P.; Kjær, K. S.; van Driel, T. B.; Mars, J.; Ochsmann, J. W.; Pontoni, D.; Deutsch, M.; Nielsen, M. M.; Mezger, M. Molecular Scale Structure and Dynamics at an Ionic Liquid/Electrode Interface. *Faraday Discuss.* **2018**, *206*, 141–157.

(18) Bovio, S.; Podestà, A.; Milani, P.; Ballone, P.; Del Popolo, M. G. Nanometric Ionic-liquid Films on Silica: a Joint Experimental and Computational Study. *J. Phys.-Condes. Matter* **2009**, *21*.

(19) Yokota, Y.; Harada, T.; Fukui, K. Direct Observation of Layered Structures at Ionic Liquid/Solid Interfaces by Using Frequency-modulation Atomic Force Microscopy. *Chem. Commun.* **2010**, *46*, 8627–8629.

(20) Comtet, J.; Nigues, A.; Kaiser, V.; Coasne, B.; Bocquet, L.; Siria, A. Nanoscale Capillary Freezing of Ionic Liquids Confined Between Metallic Interfaces and the Role of Electronic Screening. *Nat. Mater.* **2017**, *16*, 634–639.

(21) Bou-Malham, I.; Bureau, L. Nanoconfined Ionic Liquids: Effect of Surface Charges on Flow and Molecular Layering. *Soft Matter* **2010**, *6*, 4062–4065.

(22) Ueno, K.; Kasuya, M.; Watanabe, M.; Mizukami, M.; Kurihara, K. Resonance Shear Measurement of Nanoconfined Ionic Liquids. *Phys. Chem. Chem. Phys.* **2010**, *12*, 4066–4071.

(23) Lhermerout, R.; Perkin, S. Nanoconfined Ionic Liquids: Disentangling Electrostatic and Viscous Forces. *Phys. Rev. Fluids* **2018**, *3*, 014201(1–13).

(24) Sha, M.; Wu, G.; Dou, Q.; Tang, Z.; Fang, H. Double-Layer Formation of [Bmim][PF6] Ionic Liquid Triggered by Surface Negative Charge. *Langmuir* **2010**, *26*, 12667–12672.

(25) Dou, Q.; Sha, M.; Fu, H.; Wu, G. Mass Distribution and Diffusion of [1-Butyl-3-methylimidazolium][Y] Ionic Liquids Adsorbed on the Graphite Surface at 300-800 K. *ChemPhysChem* **2010**, *11*, 2438–2443.

(26) Yokota, Y.; Miyamoto, H.; Imanishi, A.; Inagaki, K.; Morikawa, Y.; Fukui, K.-i. Structural and Dynamic Properties of 1-butyl-3-methylimidazolium Bis(Trifluoromethanesulfonyl) Imide/Mica and Graphite Interfaces Revealed by Molecular Dynamics Simulation. *Phys. Chem. Chem. Phys.* **2018**, *20*, 6668–6676.

(27) Gil, P. S.; Jorgenson, S. J.; Riet, A. R.; Lacks, D. J. Relationships between Molecu-

lar Structure, Interfacial Structure, and Dynamics of Ionic Liquids near Neutral and Charged Surfaces. *J. Phys. Chem. C* **2018**, *122*, 27462–27468.

(28) Ntim, S.; Sulpizi, M. Role of Image Charges in Ionic Liquid Confined between Metallic Interfaces. *Phys. Chem. Chem. Phys.* **2020**, *22*, 10786–10791.

(29) Kislenko, S. A.; Amirov, R. H.; Samoylov, I. S. Influence of temperature on the structure and dynamics of the [BMIM][PF6] ionic liquid/graphite interface. *Phys. Chem. Chem. Phys.* **2010**, *12*, 11245–11250.

(30) Lockett, V.; Sedev, R.; Ralston, J.; Horne, M.; Rodopoulos, T. Differential Capacitance of the Electrical Double Layer in Imidazolium-based Ionic Liquids: Influence of Potential, Cation Size, and Temperature. *J. Phys. Chem. C* **2008**, *112*, 7486–7495.

(31) Gore, T. R.; Bond, T.; Zhang, W.; Scott, R. W. J.; Burgess, I. J. Hysteresis in the Measurement of Double-layer Capacitance at the Gold-ionic Liquid Interface. *Electrochem. Commun.* **2010**, *12*, 1340–1343.

(32) Drüschler, M.; Huber, B.; Passerini, S.; Roling, B. Hysteresis Effects in the Potential-Dependent Double Layer Capacitance of Room Temperature Ionic Liquids at a Polycrystalline Platinum Interface. *J. Phys. Chem. C* **2010**, *114*, 3614–3617.

(33) Pajkossy, T.; Kolb, D. M. The Interfacial Capacitance of Au(100) in an Ionic Liquid, 1-Butyl-3-methyl-imidazolium Hexafluorophosphate. *Electrochem. Commun.* **2011**, *13*, 284–286.

(34) Alam, M. T.; Masud, J.; Islam, M. M.; Okajima, T.; Ohsaka, T. Differential Capacitance at Au(111) in 1-Alkyl-3-methylimidazolium Tetrafluoroborate Based Room-Temperature Ionic Liquids. *J. Phys. Chem. C* **2011**, *115*, 19797–19804.

(35) Roling, B.; Drüschler, M.; Huber, B. Slow and Fast Capacitive Process Taking Place at the Ionic Liquid/electrode Interface. *Faraday Discuss.* **2012**, *154*, 303–311.

(36) Singh, M. B.; Kant, R. Theory for Anomalous Electric Double-Layer Dynamics in Ionic Liquids. *J. Phys. Chem. C* **2014**, *118*, 8766–8774.

(37) Makino, S.; Kitazumi, Y.; Nishi, N.; Kakiuchi, T. Charging Current Probing of the Slow Relaxation of the Ionic Liquid Double Layer at the Pt Electrode. *Electrochem. Commun.* **2011**, *13*, 1365–1368.

(38) Sebastian, P.; Sandoval, A. P.; Climent, V.; Feliu, J. M. Study of the Interface Pt(111)/[Emmim][Ntf2] Using Laser-induced Temperature Jump Experiments. *Electrochem. Commun.* **2015**, *55*, 39–42.

(39) Zhou, W.; Inoue, S.; Iwahashi, T.; Kanai, K.; Seki, K.; Miyamae, T.; Kim, D.; Katayama, Y.; Ouchi, Y. Double layer structure and adsorption/desorption hysteresis of neat ionic liquid on Pt electrode surface - an in-situ IR-visible sum-frequency generation spectroscopic study. *Electrochem. Commun.* **2010**, *12*, 672–675.

(40) Motobayashi, K.; Minami, K.; Nishi, N.; Sakka, T.; Osawa, M. Hysteresis of Potential-Dependent Changes in Ion Density and Structure of an Ionic Liquid on a Gold Electrode: In Situ Observation by Surface-Enhanced Infrared Absorption Spectroscopy. *J. Phys. Chem. Lett.* **2013**, *4*, 3110–3114.

(41) Nishi, N.; Minami, K.; Motobayashi, K.; Osawa, M.; Sakka, T. Interfacial Structure at the Quaternary Ammonium-Based Ionic Liquids vertical bar Gold Electrode Interface Probed by Surface-Enhanced Infrared Absorption Spectroscopy: Anion Dependence of the Cationic Behavior. *J. Phys. Chem. C* **2017**, *121*, 1658–1666.

(42) Motobayashi, K.; Nishi, N.; Inoue, Y.; Minami, K.; Sakka, T.; Osawa, M. Potential-induced Restructuring Dynamics of Ionic Liquids on a Gold Electrode: Steric Effect of Constituent Ions Studied by Surface-enhanced Infrared Absorption Spectroscopy. *J. Electroanal. Chem.* **2017**, *800*, 126–133.

(43) Voegeli, W.; Arakawa, E.; Matsushita, T.; Sakata, O.; Wakabayashi, Y. Dynamical Response of the Electric Double Layer Structure of the DEME-TFSI Ionic Liquid to Potential Changes Observed by Time-Resolved X-ray Reflectivity. *Z. Phys. Chem.* **2016**, *230*, 577–585.

(44) Nishi, N.; Hirano, Y.; Motokawa, T.; Kakiuchi, T. Ultraslow Relaxation of the Structure at the Ionic Liquid|Gold Electrode Interface to a Potential Step Probed by Electrochemical Surface Plasmon Resonance Measurements: Asymmetry of the Relaxation Time to the Potential-Step Direction. *Phys. Chem. Chem. Phys.* **2013**, *15*, 11615–11619.

(45) Nishi, N.; Ikeda, Y.; Sakka, T. Electrochemical Surface Plasmon Resonance as a Probe of Redox Reactions at the Ionic Liquid|Gold Interface. *J. Electroanal. Chem.* **2018**, *817*, 210–216.

(46) Zhang, S.; Nishi, N.; Sakka, T. Electrochemical Surface Plasmon Resonance Measurements of Camel-Shaped Static Capacitance and Slow Dynamics of Electric Double Layer Structure at the Ionic Liquid/Electrode Interface. *J. Chem. Phys.* **2020**, *153*, 044707(1–7).

(47) Harrick, N.; Loeb, G. Multiple Internal Reflection Fluorescence Spectrometry. *Anal. Chem.* **1973**, *45*, 687–691.

(48) Garrison, M.; Iuliano, D.; Saavedra, S.; Truskey, G.; Reichert, W. Postadsorption Changes in the Emission Maximum of Acrylodan-labeled Bovine Serum-albumin Using Total Internal-Reflection Fluorescence. *J. Colloid Interface Sci.* **1992**, *148*, 415–424.

(49) Phimphivong, S.; Saavedra, S. Terbium Chelate Membrane Label for Time-resolved, Total Internal Reflection Fluorescence Microscopy of Substrate-adherent Cells. *Bioconjugate Chem.* **1998**, *9*, 350–357.

(50) Ishizaka, S.; Nakatani, K.; Habuchi, S.; Kitamura, N. Total Internal Reflection Fluorescence Dynamic Anisotropy of Sulforhodamine 101 at a Liquid/Liquid Interface:

Rotational Reorientation times and Interfacial Structures. *Anal. Chem.* **1999**, *71*, 419–426.

(51) Tsukahara, S.; Yamada, Y.; Watarai, H. Effect of Surfactants on In-plane and Out-of-plane Rotational Dynamics of Octadecylrhodamine B at Toluene-water Interface. *Langmuir* **2000**, *16*, 6787–6794.

(52) Reichert, W.; Truskey, G. Total Internal-reflection Fluorescence (TIRF) Microscopy. 1. Modeling Cell Contact Region Fluorescence. *J. Cell Sci.* **1990**, *96*, 219–230.

(53) Axelrod, D. Total Internal Reflection Fluorescence Microscopy in Cell Biology. *Methods Enzymol.* **2003**, *361*, 1–33.

(54) Yasui, Y.; Kitazumi, Y.; Ishimatsu, R.; Nishi, N.; Kakiuchi, T. Ultraslow Response of Interfacial Tension to the Change in the Phase-Boundary Potential at the Interface between Water and a Room-Temperature Ionic Liquid, Trioctylmethylammonium bis(nonafluorobutanesulfonyl)amide. *J. Phys. Chem. B* **2009**, *113*, 3273–3276.

(55) Yasui, Y.; Kitazumi, Y.; Nishi, N.; Kakiuchi, T. Electrocapillarity under Ultraslow Relaxation of the Ionic Liquid Double Layer at the Interface between Trioctylmethylammonium Bis(nonafluorobutanesulfonyl)amide and Water. *J. Phys. Chem. B* **2010**, *114*, 11141–11148.

(56) Kakiuchi, T.; Yasui, Y.; Kitazumi, Y.; Nishi, N. Voltammetric Manifestation of the Ultraslow Dynamics at the Interface between Water and an Ionic Liquid. *ChemPhysChem* **2010**, *11*, 2912–2918.

(57) Yasui, Y.; Kitazumi, Y.; Mizunuma, H.; Nishi, N.; Kakiuchi, T. A Comparison of the Ultraslow Relaxation Processes at the Ionic Liquid|Water Interface for Three Hydrophobic Ionic Liquids. *Electrochem. Commun.* **2010**, *12*, 1479–1482.

(58) Iwaki, S., Ph.D. thesis, Graduate School of Pharmaceutical Sciences, The University of Tokyo, 2015.

(59) Tredwell, C.; Osborne, A. Viscosity Dependent Internal-Conversion in the Rhodamine Dye, Fast Acid Violet-2R. *J. Chem. S., Faraday Trans.* **1980**, *76*, 1627–1637.

(60) Osborne, A.; Winkworth, A. Viscosity-Dependent Internal-Conversion in an Aryl-Substituted Rhodamine Dye. *Chem. Phys. Lett.* **1982**, *85*, 513–517.

(61) Nishi, N.; Murakami, H.; Yasui, Y.; Kakiuchi, T. Use of Highly Hydrophobic Ionic Liquids for Ion-selective Electrodes of the Liquid Membrane Type. *Anal. Sci.* **2008**, *24*, 1315–1320.

(62) Nishi, N.; Kasuya, K.; Kakiuchi, T. Surface Structure of a Hydrophobic Ionic Liquid Probed by Spectroscopic Ellipsometry. *J. Phys. Chem. C* **2012**, *116*, 5097–5102.

(63) Nishi, N.; Uchiyashiki, J.; Oogami, R.; Sakka, T. Ionic Liquid Structure at the Electrified Ionic Liquid|Hg Interface Studied Using in situ Spectroscopic Ellipsometry. *Thin Solid Films* **2014**, *571*, 735–738.

(64) Papirer, E., Ed. *Adsorption on Silica Surfaces*; Marcel Dekker: New York, 2000.

(65) Würth, C.; Grabolle, M.; Pauli, J.; Spieles, M.; Resch-Genger, U. Relative and Absolute Determination of Fluorescence Quantum Yields of Transparent Samples. *Nat. Protoc.* **2013**, *8*, 1535–1550.

(66) Förster, T.; Hoffmann, G. Die Viskositätsabhängigkeit der Fluoreszenzquantenausbeuten einiger Farbstoffsysteme. *Z. Phys. Chem.* **1971**, *75*, 63–76.

(67) Mercade-Prieto, R.; Rodriguez-Rivera, L.; Chen, X. D. Fluorescence Lifetime of Rhodamine B in Aqueous Solutions of Polysaccharides and Proteins as a Function of Viscosity and Temperature. *Photochem. Photobiol. Sci.* **2017**, *16*, 1727–1734.

(68) Karstens, T.; Kobs, K. Rhodamine-B and Rhodamine-101 as Reference Substances for Fluorescence Quantum Yield Measurements. *J. Phys. Chem.* **1980**, *84*, 1871–1872.

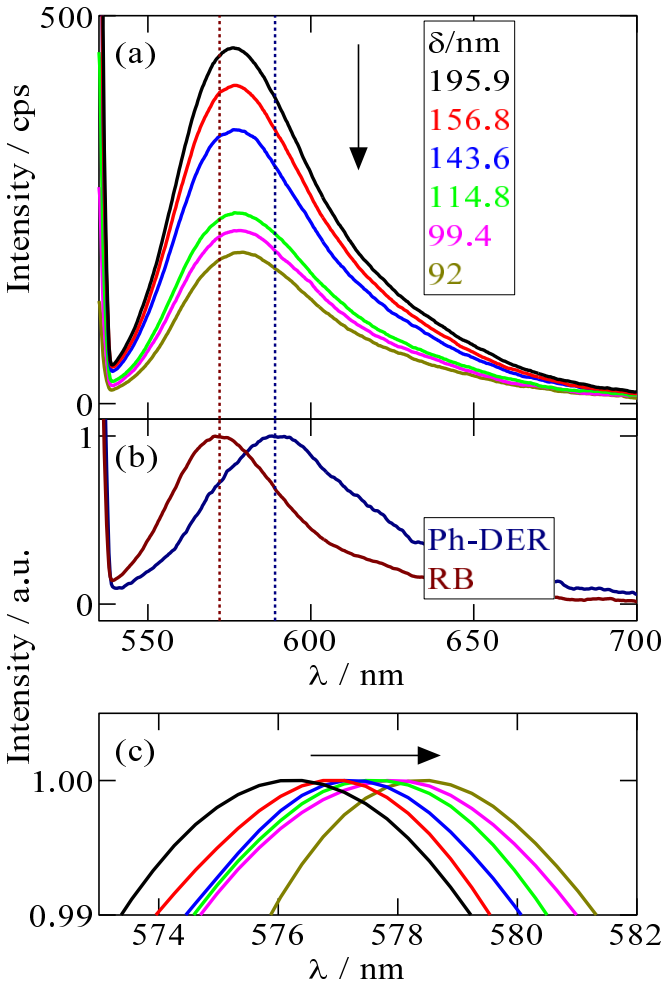

Fig.1. (a) TIRF spectra of Ph-DER (10 μM) and RB (0.5 μM) simultaneously dissolved in TOMAC4C4N at various δ and (b) TIRF spectrum of each dye in TOMAC4C4N. The dotted lines are the fluorescence maximum wavelength for Ph-DER and RB. (c) Normalized TIRF spectra shown in (a).

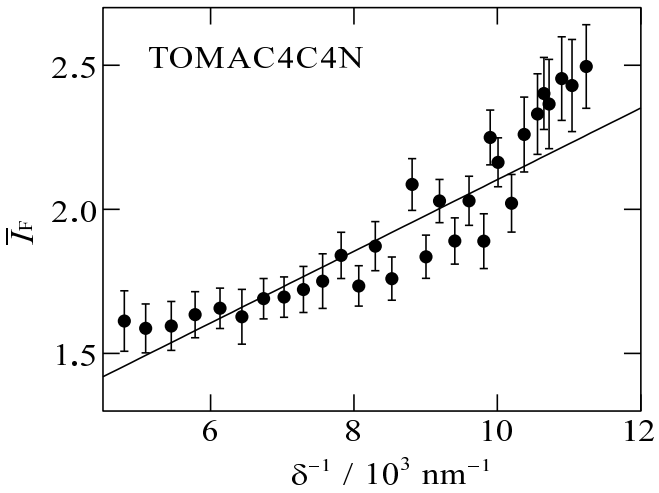

Fig.2. $\bar{I}_{\rm F}$ vs δ^{-1} plots for TOMAC4C4N. The error bars are the standard errors from CLS. The solid line is the fitted line using eq 4 with $d(f-1) = 72 \pm 16$ nm.

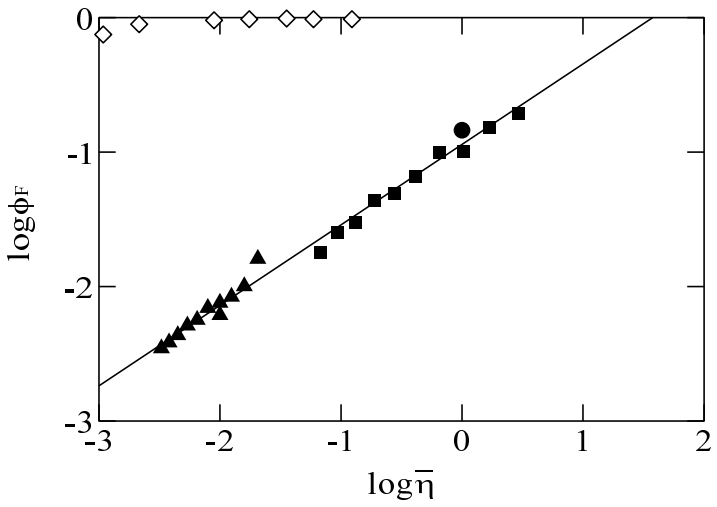

Fig.3. Experimental plots of $\log\phi_{\rm F}$ vs $\log\bar{\eta}$ for Ph-DER in TOMAC4C4N (circle), glycerol (square), and ethylene glycol (triangle) at various temperatures from 5 to 50°C for the latter two. The horizontal axis $\bar{\eta}$ is η normalized with that for TOMAC4C4N at 20°C (2000 mPa s). The solid line is the linear regression line. The data for RB (open diamond) was taken from Ref.[68] in ethanol at various temperatures.

Graphical TOC Entry